



# Fermi National Accelerator Laboratory

FERMILAB-Pub-81/30-EXP  
7420.180  
(Submitted to Nucl. Phys. B)

## QUARK JETS FROM ANTINEUTRINO INTERACTIONS III; TRANSVERSE STRUCTURE OF THE QUARK JETS

J. P. Berge, D. Bogert, R. Endorf\*, R. Hanft, J. A. Malko  
F. A. Nezrick, and R. Orava†  
Fermi National Accelerator Laboratory  
Batavia, Illinois 60510 USA

and

V. I. Efremenko, A. V. Fedotov, P. A. Gorichev, V. S. Kaftanov,  
G. K. Kliger, V. Z. Kolganov, S. P. Krutchinin, M. A. Kubantsev,  
I. V. Makhljueva, V. I. Shekeljan, and V. G. Schevchenko  
Institute for Theoretical and Experimental Physics  
Moscow, USSR

and

V. V. Ammosov, A. G. Denisov, G. S. Gapienko, V. A. Gapienko,  
V. I. Klukhin, V. I. Koreshev, P. V. Pitukhin, V. I. Sirotenko,  
E. A. Slobodyuk, Z. V. Usubov, and V. G. Zaetz  
Institute of High Energy Physics, Serpukhov, USSR

and

J. Bell, C. T. Coffin, B.P. Roe, and D. Sinclair  
University of Michigan  
Ann Arbor, Michigan 48104 USA

May 1981

\*Visitor from the University of Cincinnati, Cincinnati, Ohio  
†Robert R. Wilson Fellow at Fermilab. On leave from the  
University of Helsinki, Helsinki, Finland



## ABSTRACT

We extend our systematic study of the properties of hadron jets produced in antineutrino-nucleon charged current interactions to those observables which characterize the distribution of particles perpendicular to the jet axis.

These antineutrino induced jets are found to have properties similar to those of the jets observed in  $e^+e^-$  annihilation at comparable center-of-mass energies. No deviations from the simple quark-parton model predictions are found.

## 1. Introduction

Well collimated showers of hadrons are frequently observed in deeply inelastic lepton-nucleon interactions and in  $e^+e^-$  annihilation experiments. These showers, or jets, which consist of hadrons with transverse momenta limited to a few hundred MeV/c relative to the jet direction, appear to have the same basic longitudinal structure in all hard scattering processes.<sup>1-3</sup>

In the quark-parton picture of deeply inelastic lepton-nucleon scattering a pointlike interaction occurs between the weak current and a parton with a "primordial" transverse momentum,  $k_t$ , relative to the current direction (Fig. 1).<sup>4</sup> The hadron jet arises from quark "hadronization" and moves along the fragmenting quark direction. The quark jet direction may differ from the current direction because of the primordial transverse motion of the struck quark. It is thought that  $e^+e^-$  annihilation to hadrons proceeds via production of a quark-antiquark pair with no primordial  $k_t$ . The quark and antiquark subsequently fragment to produce the observed hadron momentum spectra in  $e^+e^-$  experiments. We can get a measure of  $k_t$  by comparing our results with  $e^+e^-$  data provided gluon bremsstrahlung can be adequately accounted for. However, hard gluon bremsstrahlung from the outgoing quark could also lead to jets from lepton-nucleon interactions having different shapes than jets from  $e^+e^-$  annihilation.<sup>5,6</sup>

In this article we study the transverse momentum structure of hadron jets produced in charged current antineutrino interactions. We investigate uncertainties related to the determination of the jet axis and compare thrust, sphericity and angular

energy flow for our jet data with the corresponding quantities measured in  $e^+e^-$  annihilation experiments and in other anti-neutrino (neutrino) experiments.

## 2. Experimental procedure

Our analysis is based on data obtained in a wide-band anti-neutrino beam exposure of the Fermilab 15-foot bubble chamber filled with a 64% atomic neon-hydrogen mixture.

A sample of 4600 charged current antineutrino-nucleon interactions fulfilled these criteria: (1) incident antineutrino energy  $E_{\bar{\nu}} > 10$  GeV ( $E_{\bar{\nu}}$  is defined as the sum of the outgoing muon energy and the reconstructed hadronic energy in an event); (2) muon laboratory momentum  $p_{\mu} > 4$  GeV/c (the muon is identified by the External Muon Identifier supplemented by a kinematical procedure);<sup>7</sup> (3) lepton four-momentum transfer squared  $Q^2 > 1$  GeV<sup>2</sup>/c<sup>2</sup>; and (4) hadronic center-of-mass energy  $W > 2$  GeV.<sup>8</sup> Selection criteria 3 and 4 are applied to eliminate quasi-elastic channels. The reader interested in more complete experimental details is referred to Ref. 7.

We require that the charged hadron tracks be well measured; the relative error in the measured hadron momentum is  $\Delta p/p < 30\%$ . To account for the interactions which occur close to the main interaction point we use a weighting procedure.<sup>9</sup> All protons stopping in the chamber with momentum below 1 GeV/c are identified and removed from the track sample in each event; the pion mass is assigned to each of the remaining tracks. In order to

compare our results with the  $e^+e^-$  or neutrino-hydrogen data<sup>10,11</sup> an additional selection criterion is needed; the charged hadron multiplicity,  $n_{ch}$ , is required to be larger than four.

In this experiment we measured neutral stars from neutral particle interactions and  $e^+e^-$  pairs from photon conversions, and this information was used in determination of  $Q^2$  and  $W^2$ . However, we can not in general reconstruct the momenta of individual neutral hadrons, therefore the distributions from this experiment presented below contain only charged hadrons. We note that recent  $e^+e^-$  data available for comparison likewise include only charged hadrons. There are some comparisons of  $e^+e^-$  data with and without neutrals which indicate that the omission of neutrals is unimportant.<sup>2</sup>

We investigated uncertainties related to the finite experimental resolution and measurement systematics of our experiment by using a Monte Carlo program<sup>12</sup> which is specially designed to meet our experimental conditions. In the model a particular hadronic final state is generated according to a longitudinal phase space (LPS) construction with  $d\sigma/dp_T^2 \propto \exp[-b(m^2 + p_T^2)^{1/2}]$ . Hadron multiplicities are parametrized as a function of  $W$  according to our experimental results. Effects caused by wrong mass assignments in the kinematical variables for the misidentified mesons and fast (momentum larger than 1 GeV/c in laboratory) protons are studied by using the measured spectra of identified neutral strange particles.

### 3. Jet axes

#### 3.1 Definitions

The two popular variables for defining the jet axis, thrust and sphericity, were originally designed for  $e^+e^-$  jets where there is no *a priori* knowledge of the quark jet direction. In leptonproduction experiments there are additional possibilities for studying the jet shape, such as distributions relative to the lepton momentum transfer direction,  $\vec{Q}$ , and relative to the normal to the lepton plane. In the following, we shall investigate uncertainties related to the different choices of the jet axis.

The maximum directed momentum in the final state is the thrust variable,<sup>13</sup>  $T$ , that is defined for any axis,  $\vec{i}$ , in the event sphere by

$$T = \frac{\sum_{k=1}^{n_{ch}} (\vec{p}_k \cdot \vec{i})}{\sum_{k=1}^{n_{ch}} |\vec{p}_k|}, \quad (1)$$

where the summation is over all charged hadrons in the event and  $\vec{p}_k$ , is the hadron momentum vector in the hadronic c.m.s.<sup>14</sup> The thrust axis,  $\vec{i}_T$ , is therefore the axis which maximizes  $T$ . For the "jet-like" events in which the hadrons are collimated in two narrow cones the thrust variable is large ( $T \rightarrow 1$ ), whereas in isotropic events  $T = 1/2$ . The function (1) is maximized for each event to determine the thrust axis,  $\vec{i}_T$ , and the magnitude of the thrust variable,  $T$ .

We define the sphericity variable,<sup>15</sup>  $S$ , associated with an arbitrary axis  $\vec{i}$  by

$$S = \frac{\sum_{k=1}^{n_{ch}} (\vec{p}_k \times \vec{i})^2}{\sum_{k=1}^{n_{ch}} |\vec{p}_k|^2}. \quad (2)$$

The axis which minimizes  $S$  is the sphericity axis,  $\vec{i}_S$ . For the "jet-like" events sphericity is small ( $S \rightarrow 0$ ) and for the isotropic events  $S$  is large ( $S=1$ ).

### 3.2 Uncertainties

The difference between the thrust and sphericity axes is a measure of the uncertainty in the determination of the jet direction.

From our previous analysis on net charge of the jets we expect that at sufficiently high hadron c.m.s energies ( $W \gtrsim 8$  GeV) the small overlap between the current and target fragmentation regions would allow an adequate determination of the initial fragmenting quark direction as the thrust or sphericity axis. At low c.m.s energies ( $W \lesssim 3$  GeV) ambiguity between the current and target fragments should prevent a meaningful analysis of the jet shape.<sup>7</sup>

In antineutrino (neutrino) - nucleon interactions the current direction,  $\vec{i}_Q = (\vec{p}_{\bar{\nu}, \nu} - \vec{p}_\mu) / |(\vec{p}_{\bar{\nu}, \nu} - \vec{p}_\mu)|$ , is smeared because of the limited  $\bar{\nu}(\nu)$  momentum resolution. The lepton plane determined by the directions of the incoming antineutrino

(neutrino) and the outgoing muon is, however, precisely known. We define  $\vec{i}_{\mu\nu}$ , as a unit vector in this plane and study correlations between the directions  $\vec{i}_T$ ,  $\vec{i}_S$ ,  $\vec{i}_Q$ , and  $\vec{i}_{\mu\nu}$  in antineutrino (neutrino) experiments. We also compare our results on thrust and sphericity axes with the results obtained in  $e^+e^-$  experiments.

Distributions of  $\cos(\vec{i}_T, \vec{i}_S)$ ,  $\cos(\vec{i}_T, \vec{i}_Q)$ ,  $\cos(\vec{i}_S, \vec{i}_Q)$ ,  $\cos(\vec{i}_T, \vec{i}_{\mu\nu})$  and  $\cos(\vec{i}_S, \vec{i}_{\mu\nu})$ , where  $(\vec{i}_1, \vec{i}_2)$  denotes the angle between any pair of the axes listed above, are shown in Fig. 2 for the two c.m.s energy intervals:  $2 < W < 3$  GeV ( $\langle W \rangle = 2.5$  GeV for the filled circles) and  $W > 8.5$  GeV ( $\langle W \rangle = 10.5$  GeV for the open circles). These distributions show that for a majority of the events the different choices for the jet axes coincide at large c.m.s energies. The average angle between each pair of the axes is plotted in Fig. 3 as a function of  $W$ . At small c.m.s energies the current direction ( $\vec{i}_Q$ ) often differs significantly from the thrust ( $\vec{i}_T$ ) and sphericity ( $\vec{i}_S$ ) axes. The thrust axis and the sphericity axis are strongly correlated already at low c.m.s energies (Fig. 3a), whereas a significant correlation between the pairs  $(\vec{i}_T, \vec{i}_Q)$  and  $(\vec{i}_S, \vec{i}_Q)$  is present only at the highest  $W$ -values. The correlation between the pairs  $(\vec{i}_T, \vec{i}_{\mu\nu})$  and  $(\vec{i}_S, \vec{i}_{\mu\nu})$  becomes significant at the c.m.s energies of  $W > 4$  GeV (Fig. 3b).

We compare in Fig. 3a our observations with the results obtained in a  $e^+e^-$  experiment<sup>16</sup> and in another antineutrino-nucleon experiment<sup>10</sup> and find good agreement between the results

obtained for the average angle between the thrust and sphericity axis,  $\langle(\vec{i}_T, \vec{i}_S)\rangle$ .

Dependence of the axes  $\vec{i}_T$ ,  $\vec{i}_S$ , and  $\vec{i}_{\mu\nu}$  on the direction of the fastest charged particle in the jet,  $\vec{i}_f$ , is studied in Fig. 4 as a function of  $W$ . The average angle between each pair of axes:  $(\vec{i}_f, \vec{i}_T)$ ,  $(\vec{i}_f, \vec{i}_S)$  and  $(\vec{i}_f, \vec{i}_{\mu\nu})$  is observed to decrease as a function of  $W$  for  $W > 4$  GeV. A similar average angle at a single fixed c.m.s energy, was obtained in the  $e^+e^-$  experiment<sup>16</sup> and in the antineutrino-hydrogen experiment<sup>10</sup> (Fig. 4). For  $W > 4$  GeV, the different choices for jet axis agree within  $20^\circ$ , and we therefore consider  $\vec{i}_T$  and  $\vec{i}_S$  as reasonable measures of the true jet axis as well as  $\vec{i}_{\mu\nu}$ . In the following we will study the transverse properties of the jets with respect to the three choices for the jet axis  $\vec{i}_T$ ,  $\vec{i}_S$  and  $\vec{i}_{\mu\nu}$ .

#### 4. Transverse Structure of the Jets

##### 4.1 Transverse momentum distributions

To investigate the transverse structure of the hadron showers we first measure the hadron transverse momentum distributions relative to the different jet axes ( $\vec{i}_T$ ,  $\vec{i}_S$ , and  $\vec{i}_{\mu\nu}$ ) and secondly the thrust and sphericity distributions which describe the shape of the entire hadronic system produced in an event. In the following we shall consider only charged particles traveling forward in the hadronic c.m.s, such as those in the case previously presented as evidence for the d-quark origin of these hadrons in  $\bar{\nu}_\mu N$  charged current interactions.<sup>7</sup>

Results for average transverse momentum squared relative to the thrust axis,  $\langle p_T^2 \rangle$ , and relative to the  $\mu\nu$ -plane,  $\langle p_{out}^2 \rangle$ , are

shown in Fig. 5 as functions of the c.m.s energy. Measurements of  $\langle p_T^2 \rangle$  in  $e^+e^-$  jets<sup>2</sup> are also shown in Fig. 5; the  $\nu_\mu N$  data are seen to resemble closely the  $e^+e^-$  jets. Also shown in Fig. 5 are the predictions of our LPS model given by the solid curves. The LPS predictions agree well with the  $\nu_\mu N$  and  $e^+e^-$  results. This LPS model reproduces the  $W$  dependence of both  $\langle p_T^2 \rangle$  and  $\langle p_{out}^2 \rangle$ , and there is no evidence for additional QCD effects such as might be expected from hard gluon bremsstrahlung. The difference between the average transverse momenta  $\langle p_T^2 \rangle$  and  $\langle p_{out}^2 \rangle$  at the highest c.m.s energies where the jet axis is determined within  $10^\circ$  should measure the size of the quark primordial transverse momentum,  $\langle k_t^2 \rangle$ . In the simple quark-parton model the average transverse momentum squared of the hadrons in the jet is given as

$$2\langle p_{out}^2 \rangle = z^2 \langle k_t^2 \rangle + \langle h_T^2 \rangle, \quad (3)$$

where we have assumed that the particles in the jet are symmetrically distributed in their azimuthal angle relative to the jet axis.<sup>2</sup> The variable  $z$  is defined in the laboratory system as  $z = E_h/\nu$ , where  $E_h$  is the individual hadron energy,  $\nu = (E_\nu - E_\mu)$  and  $h_T$  is the transverse momentum gained by a hadron in the quark fragmentation process. We estimate  $\langle h_T^2 \rangle$  by utilizing Fig. 5 and Eq. (3) by choosing  $\langle h_T^2 \rangle$  to be  $\langle p_T^2 \rangle$  measured relative to the thrust axis and by using the experimentally measured average value of  $\langle z^2 \rangle = 0.14 \pm 0.01$  for  $z^2$ . We then obtain at the highest c.m.s energies ( $W \sim 10$  GeV) for  $\langle p_{out}^2 \rangle = (0.11 \pm 0.01)$  GeV<sup>2</sup>/c<sup>2</sup>,  $\langle h_T^2 \rangle = (0.160 \pm 0.005)$  GeV<sup>2</sup>/c<sup>2</sup> and thus for the quark "Fermi motion"  $\langle k_t^2 \rangle = (0.4 \pm 0.1)$  GeV<sup>2</sup>/c<sup>2</sup>. The uncertainty in

determination of  $\langle k_t^2 \rangle$  arises mainly (1) from the angular uncertainty of  $10^\circ$  in determining the jet axis and (2) from the statistical uncertainty in measuring  $\langle p_T^2 \rangle$  and  $\langle p_{out}^2 \rangle$ . Statistical uncertainty dominates the error in  $\langle k_t^2 \rangle$ . One should note here that at lower c.m.s energies the uncertainty in the determination of the jet axis is significantly larger ( $18^\circ$  at  $W \sim 4$  GeV) and the overlap between the current and target fragmentation regions prevents any meaningful attempt to measure the quark "Fermi motion". There are also uncertainties inherent in the approach used above. First, Eq. (3) should be valid at fixed  $x_B$  ( $x_B = Q^2/2Mv$ ) and  $W$ , only, whereas we integrate over  $x_B$ . We have checked the  $x_B$ -dependence of  $\langle p_T^2 \rangle$  and  $\langle p_{out}^2 \rangle$  and found that there is no significant  $x_B$ -dependence in those quantities.<sup>9</sup> Secondly, to measure the primordial momentum of a parton we should know the  $z$ -dependence of the average transverse momentum of the final state hadrons,  $\langle p_{out} \rangle$  of the final state hadrons, which exhibits the familiar seagull-effect. The seagull-effect can be partly explained by kinematics in the production process and partly by resonance production.<sup>12</sup> Transverse momentum arising from such resonance production or from the primordial motion of the fragmenting parton is generally thought to be independent of the c.m.s energy,  $W$ . One should, however, account for new thresholds introduced by charmed particle production, for example.

Another analysis utilizes exclusive neutrino-proton events to estimate quark  $\langle k_t \rangle$ .<sup>17</sup> However, these events constitute a very special sample of interactions that mainly result from

coherent processes and might not provide an adequate means for estimating  $\langle k_t \rangle$ .

#### 4.2 Thrust and sphericity distributions

Thrust and sphericity variables were invented to be used to describe the shape of an entire event in momentum space rather than to describe average characteristics of individual hadrons in the jet. We emphasize that thrust and sphericity are kinematically related to the transverse momenta of the final state hadrons and only provide another way of presenting the data.

Figure 6 shows the thrust and sphericity distributions for the two intervals of hadron c.m.s energy,  $5.5 < W < 6.7$  GeV and  $W > 8.5$  GeV, in this experiment and in the  $\bar{\nu}N$ ,  $\bar{\nu}p$ ,  $\nu p$ , and  $e^+e^-$  experiments.<sup>10,16,18,19</sup> Phenomenological (non-perturbative) model calculations<sup>6</sup> (solid curve) for quark fragmentation give a fair description of the results while the QCD calculation, without any phenomenological input to describe the parton hadronization process,<sup>20</sup> is not in agreement with the data.

The average thrust,  $\langle 1-T \rangle$ , and sphericity,  $\langle S \rangle$ , are shown in Fig. 7 as functions of the c.m.s energy for our  $\bar{\nu}N$  experiment and for the  $e^+e^-$  and other  $\bar{\nu}N(\nu N)$  experiments.<sup>10,16</sup> Good overall agreement amongst all the different data sets is observed. In the c.m.s energy region of  $W > 4$  GeV the averages  $\langle 1-T \rangle$  and  $\langle S \rangle$  fall with the increasing c.m.s energy as expected in the simple quark-parton model.

In Fig. 8 we have plotted the averages  $\langle 1-T \rangle$  and  $\langle S \rangle$  as functions of the scaling variables  $x_B$  and  $y$  ( $y = \nu/E_{\bar{\nu}}$ ) in a fixed c.m.s energy interval,  $5.5 < W < 6.7$  GeV. No significant

variation of  $\langle 1-T \rangle$  or  $\langle S \rangle$  with  $x_B$  or  $y$  is observed. We conclude that in this presently available c.m.s energy region the jet variables, thrust and sphericity, are determined by the c.m.s energy and the limited transverse momentum as suggested by kinematics and the simple quark-parton model.

### 4.3 Angular energy flow

Another measure of the angular spread of a hadron jet is the angular energy flow<sup>21</sup> with respect to the jet axis (thrust axis,  $\vec{i}_T$ ). The angular energy flow,  $d\varepsilon/d\lambda$ , is the fraction of the c.m.s energy carried by the hadrons traveling forward in the c.m.s outside a cone with the half opening angle  $\lambda$  relative to the jet axis.

In Fig. 9 we have plotted the angular energy flow for the "jet-like" events (events with  $T > 0.85$ ) in our  $\bar{\nu}_\mu N$  charged current sample. We compare our  $\bar{\nu}_\mu N$  data with  $e^+e^-$  results<sup>10,16</sup> in the same figure. The energy flow distributions are seen to be identical within the experimental accuracy. The average jet opening angle  $\langle \lambda \rangle$  as a function of thrust behaves similarly in the  $\bar{\nu}_\mu N$ ,  $\bar{\nu}_\mu p$  and  $e^+e^-$  jets as seen in Fig. 10. The average opening angle is seen to decrease rapidly with the increasing thrust.

## 5. Conclusions

In this experiment, we have investigated the transverse properties of  $\bar{\nu}_\mu N$  charged current induced jets in detail. We find that thrust and sphericity axes converge to a direction that is uniquely defined within  $10^\circ$  at  $W \sim 10$  GeV.

The transverse structure of the  $\bar{\nu}(\nu)$  charged current induced jets is explained by the simple quark-parton picture and the longitudinal phase space model without observable effects from hard gluon bremsstrahlung processes a'la QCD.

Close agreement between the transverse structure of the  $\bar{\nu}(\nu)$ -N jets and the  $e^+e^-$  jets is observed. This similarity indicates that the quark primordial motion in the target nucleon has little effect on the shape of the leptoproduced jets. The difference between the average transverse momenta measured relative to the jet axis and relative to the lepton plane in  $\bar{\nu}_\mu N$  events was used to estimate primordial transverse momentum of a quark giving a result of  $\langle k_t^2 \rangle = (0.4 \pm 0.1) \text{ GeV}^2/c^2$ .

## REFERENCES

1. M. Jacob, *Physica Scripta* **19**, 69 (1979).
2. Ch. Berger, H. Newman, G. Wolf, and S. Orito in *Proceedings of the 1979 International Symposium on Lepton and Photon Induced Interactions at High Energy*, Edited by T. Kirk and H. D. I. Abarbanel.
3. R. Orava, *Quark Jets from Deeply Inelastic Lepton Scattering*, Lectures given at The Arctic School of Physics, Lapland (1980), to be published in *Physica Scripta*.
4. See for example: R. D. Field, *Proceedings of the 15th International Conference on High Energy Physics, Tokyo (1978)* p. 743.
5. H. Georgi and H. D. Politzer, *Phys. Rev. Lett.* **40B**, 3 (1978).  
A. Mendez, *Nucl. Phys.* **B145**, 199 (1978).  
A. Mendez, *Phys. Lett.* **83B**, 331 (1978).  
E. G. Floratos, *Nuovo Cimento* **43A**, 241 (1978).  
K. H. Graid and C. H. Llewellyn Smith, *Phys. Lett.* **72B**, 34 (1978).  
G. Altarelli and G. Martinelli, *Phys. Lett.* **76B**, 89 (1978).
6. P. M. Stevenson, *Nucl. Phys.* **B156**, 43 (1979).  
P. Binet and G. Girardi, *Nucl. Phys.* **B155**, 150 (1979).
7. J. P. Berge et al., *Quark Jets from Antineutrino Interactions I; Net Charge and Factorization in the Quark Jets*, Fermilab-Pub-80/62-EXP (1980), to be published in *Nuclear Physics B*.

- V. V. Ammosov et al., Quark Jets from Antineutrino Interactions II; Inclusive Particle Spectra and Multiplicities in the Quark Jets, Fermilab-Pub-80/96-EXP (1980) (submitted to Nuclear Physics B).
8. We use the energy correction procedure described in Ref. 12 to reconstruct the hadronic and incident antineutrino energies. The following definitions of kinematical variables are used:  $\nu = E_{\bar{\nu}} - E_{\mu}$ ,  $Q^2 = 2E_{\bar{\nu}}E_{\mu}(1 - \cos\theta_{\mu})$ ,  $W^2 = M^2 + 2M\nu - Q^2$ ,  $y = \nu/E_{\bar{\nu}}$ ,  $x_B = Q^2/2M\nu$ , where  $M$  is the nucleon mass.
  9. V. V. Ammosov et al., Average transverse momentum behavior of charged hadrons in charged current  $\bar{\nu}_{\mu}N$  interactions, Serpukhov preprint IHEP-80-125 (1980).
  10. M. Derrick et al., Phys. Lett. **88B**, 177 (1979).
  11. G. Flugge, Lectures in the XVIII International Workshop, Universitat fur Kern Physik, DESY Report No. 79/26 (1979).
  12. J. Bell et al., Phys. Rev. **D19**, 1 (1979).
  13. A. DeRujula et al., Nucl. Phys. **B138**, 387 (1978)
  14. The Lorentz-transformation into the hadronic c.m.s is performed using the reconstructed value for the total hadronic energy and including the neutral particles.
  15. J. D. Bjorken and S. J. Brodsky, Phys. Rev. **D1**, 1416 (1970).
  16. Ch. Berger et al., Phys. Lett. **78B**, 176 (1978).
  17. P. Allen et al., Transverse Momentum Distributions of Hadrons in Deep Inelastic Neutrino-Proton Scattering, Oxford Preprint 83/80.

18. P. C. Bosetti et al., Nucl. Phys. B145, 13 (1979).
  19. K. Barnham et al., Sphericity and Thrust Distributions in High Energy Neutrino Interactions, CERN/EP 79-39 (1979).
  20. P. Binetruy, Phys. Lett. 91B, 295 (1980).
  21. G. Sherman and S. Weinberg, Phys. Rev. Lett. 39, 1436 (1977).
- R. D. Peccei and R. Ruckl, Energy Flow and Energy Correlations in Deep Inelastic Scattering, Preprint MPE-PAE/Pth 21/79 (1979).

FIGURE CAPTIONS

1. Schematic illustration of deep inelastic scattering: the current is absorbed by a quark with transverse motion inside the target nucleon. The quark subsequently fragments into the final state hadrons which are indicated by the arrows.
2. Angular differences (a)  $\cos(\vec{i}_T, \vec{i}_S)$ , (b)  $\cos(\vec{i}_T, \vec{i}_Q)$ , (c)  $\cos(\vec{i}_S, \vec{i}_Q)$ , (d)  $\cos(\vec{i}_T, \vec{i}_{\mu\nu})$  and (e)  $\cos(\vec{i}_S, \vec{i}_{\mu\nu})$  for the  $\bar{\nu}_\mu N$  charged current interactions in two c.m.s energy intervals:  $2 < W < 3$  GeV (solid circles), and  $W > 8.5$  GeV (open circles) with the selection  $n_{ch} > 4$  in the charged particle multiplicity.
3. Average angles (a)  $\langle(\vec{i}_T, \vec{i}_S)\rangle$ , and (b)  $\langle(\vec{i}_T, \vec{i}_Q)\rangle$ ,  $\langle(\vec{i}_S, \vec{i}_Q)\rangle$ ,  $\langle(\vec{i}_T, \vec{i}_{\mu\nu})\rangle$ ,  $\langle(\vec{i}_S, \vec{i}_{\mu\nu})\rangle$  as functions of  $W$  for  $n_{ch} > 4$ . Data from an  $e^+e^-$  experiment<sup>16</sup> and from an  $\bar{\nu}_p$  experiment<sup>10</sup> are also shown.
4. Average angles  $\langle(\vec{i}_f, \vec{i}_T)\rangle$ ,  $\langle(\vec{i}_f, \vec{i}_S)\rangle$  and  $\langle(\vec{i}_f, \vec{i}_{\mu\nu})\rangle$  as functions of  $W$  for  $n_{ch} > 4$ . Data from an  $\bar{\nu}_p$  experiment<sup>10</sup> are also shown.
5. Average transverse momentum squared of the charged hadrons in the current fragmentation region relative to the thrust axis,  $\langle p_T^2 \rangle$ , and relative to the  $\mu\nu$ -plane,  $\langle p_{out}^2 \rangle$ , as functions of  $W$ . Data from an  $e^+e^-$  experiment<sup>2</sup> are also shown. The solid curves represent predictions of a LPS model (see the text).
6. Thrust distributions for the charged hadrons in the two  $W$  regions:  $5.5 < W < 6.7$  GeV (a).  $W > 8.5$  GeV (b). and

sphericity distributions for the charged hadrons in the two  $W$  regions:  $5.5 < W < 6.7$  GeV (c),  $W > 8.5$  GeV (d). Results from an  $e^+e^-$  experiment,<sup>16</sup> from a  $\nu p$  experiment<sup>10</sup> and from a  $\nu N$  experiment<sup>19</sup> are also shown. The solid curves in a, b represent predictions of a phenomenological model,<sup>6</sup> the dashed curves in b, c result from a purely perturbative QCD calculation.<sup>20</sup>

7. Average thrust,  $\langle 1-T \rangle$ , and average sphericity,  $\langle S \rangle$ , as functions of  $W$  with  $n_{ch} > 4$ . Data from an  $e^+e^-$  experiment<sup>16</sup> and from an  $\nu p$  experiment<sup>10</sup> are also shown.
8. Average thrust,  $\langle 1-T \rangle$ , and average sphericity,  $\langle S \rangle$ , as functions of  $x_B$  and  $y$  with the selections  $5.5 < W < 6.7$  GeV,  $n_{ch} > 4$ .
9. Angular energy flow  $d\varepsilon/d\lambda$  of charged particles ( $n_{ch} > 4$ ) relative to the thrust axis as a function of the jet opening angle  $\lambda$ . Results from an  $e^+e^-$  experiment<sup>16</sup> and from an  $\nu p$  experiment<sup>10</sup> are also shown.
10. Width of the energy flow distribution as given by the average half-opening angle  $\langle \lambda \rangle$  as a function of thrust. The solid line represents  $e^+e^-$  results<sup>16</sup> and the dashed line  $\nu p$  results.<sup>10</sup>

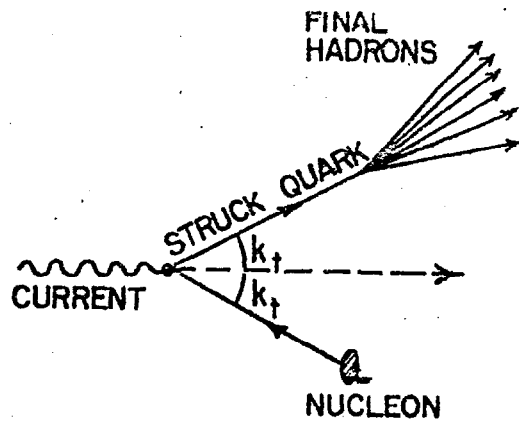


Fig. 1

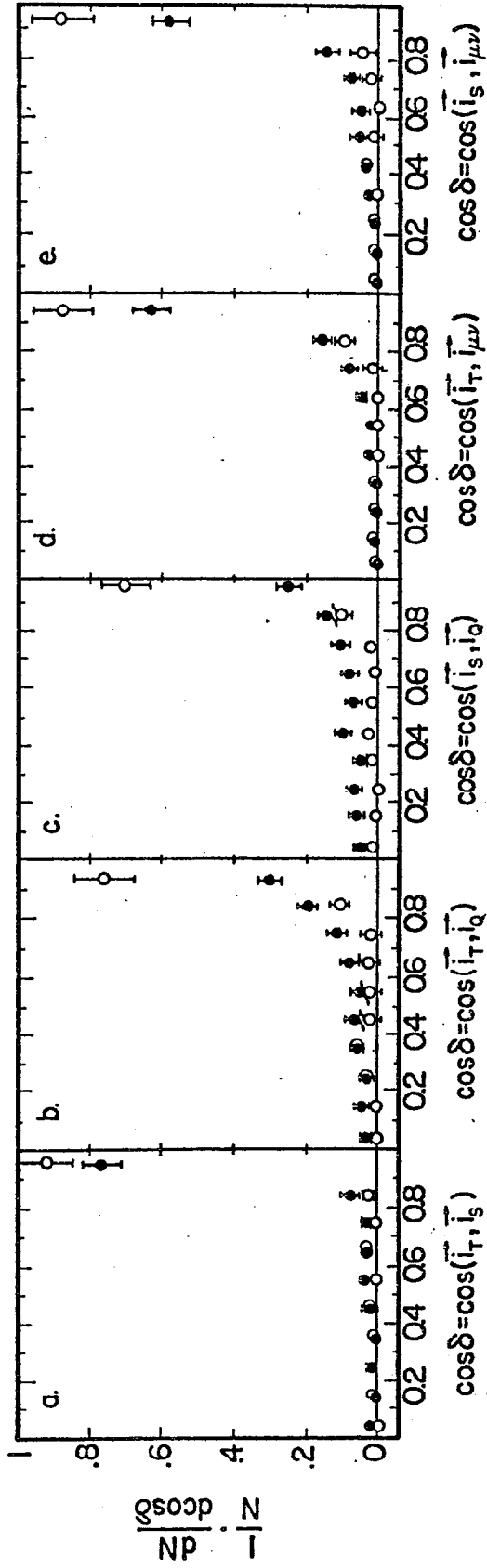


Fig. 2

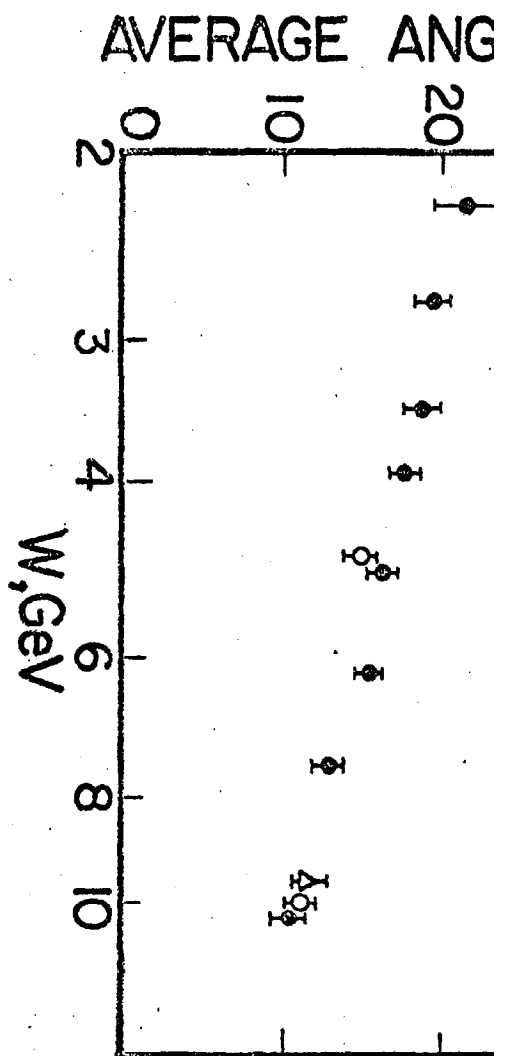


Fig. 3a

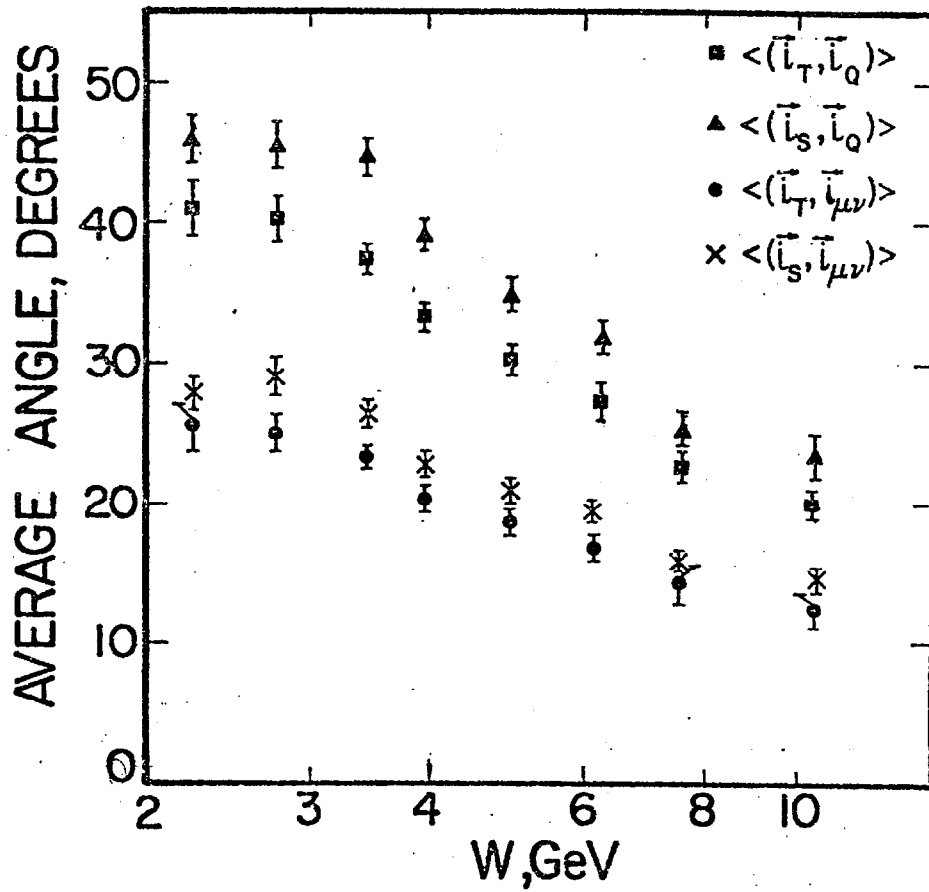


Fig. 3b

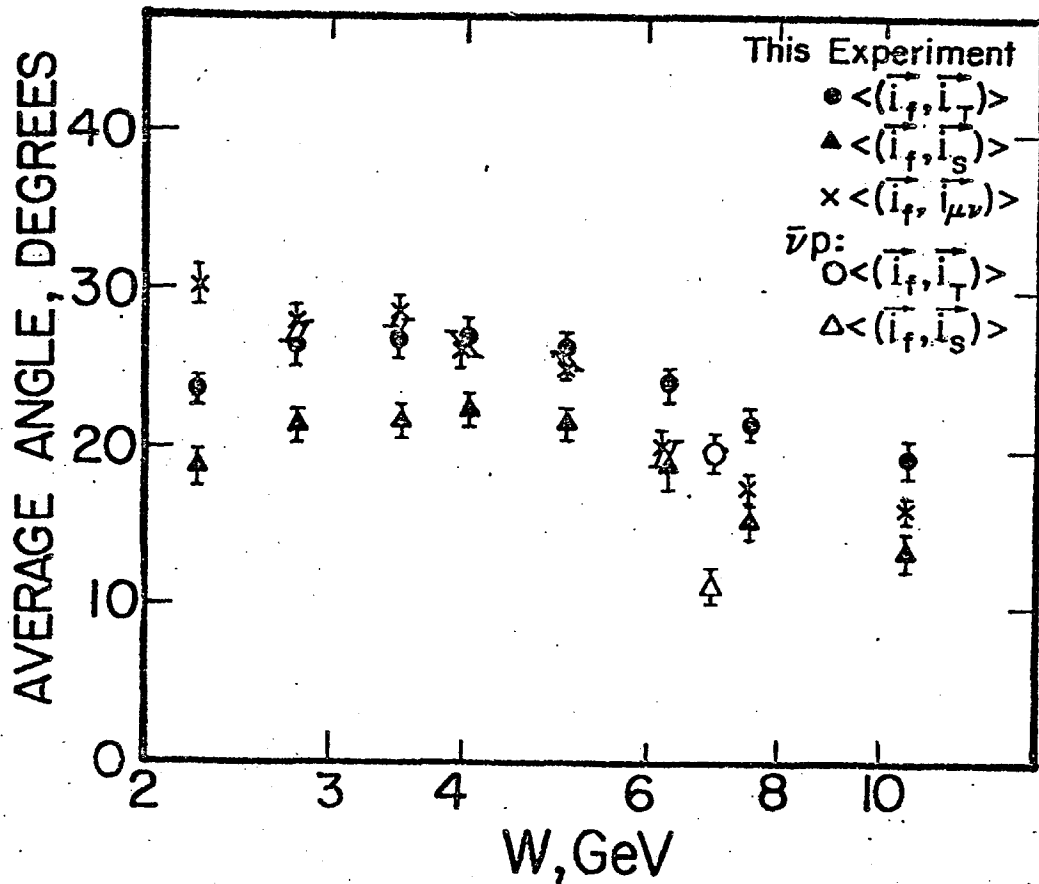


Fig. 4

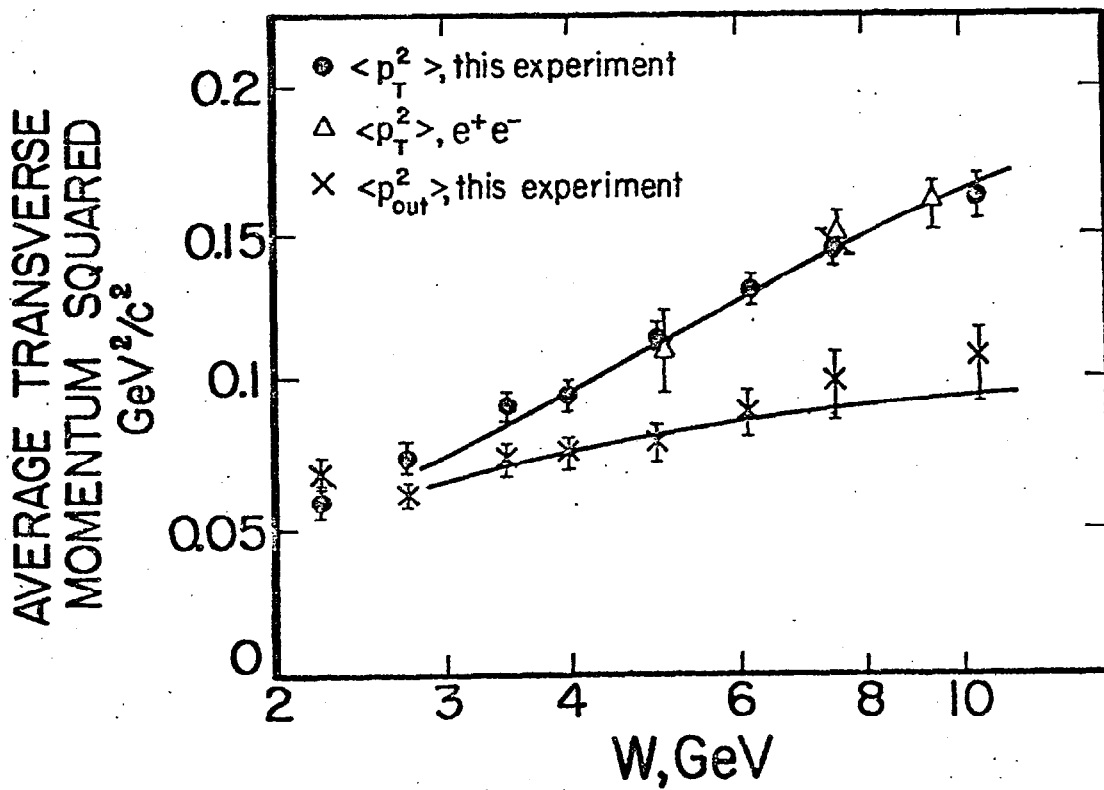


Fig. 5

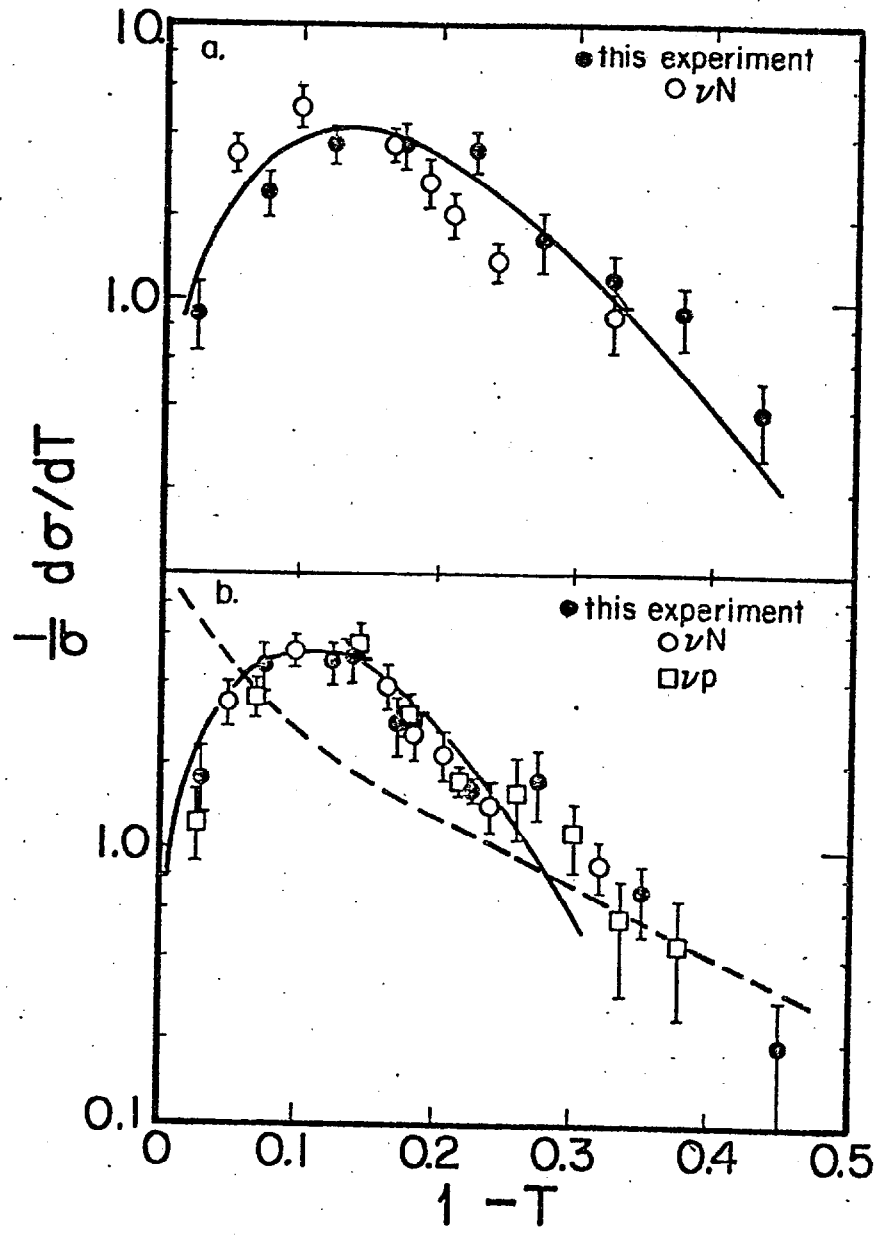


Fig. 6 a,b

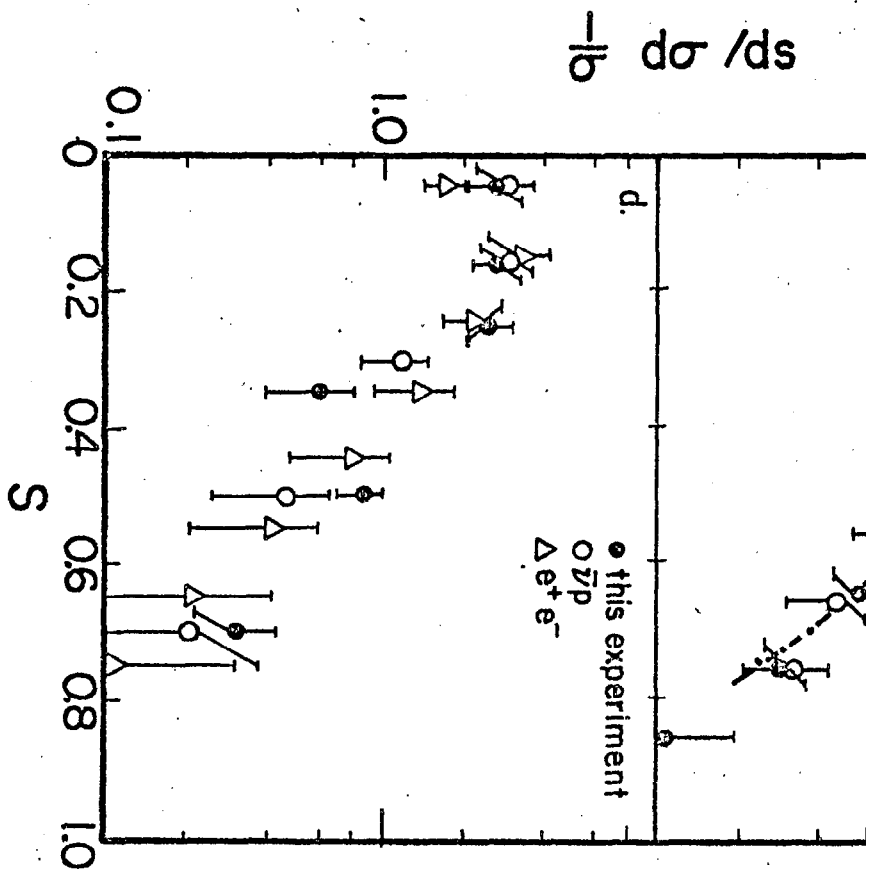


Fig.6c,d

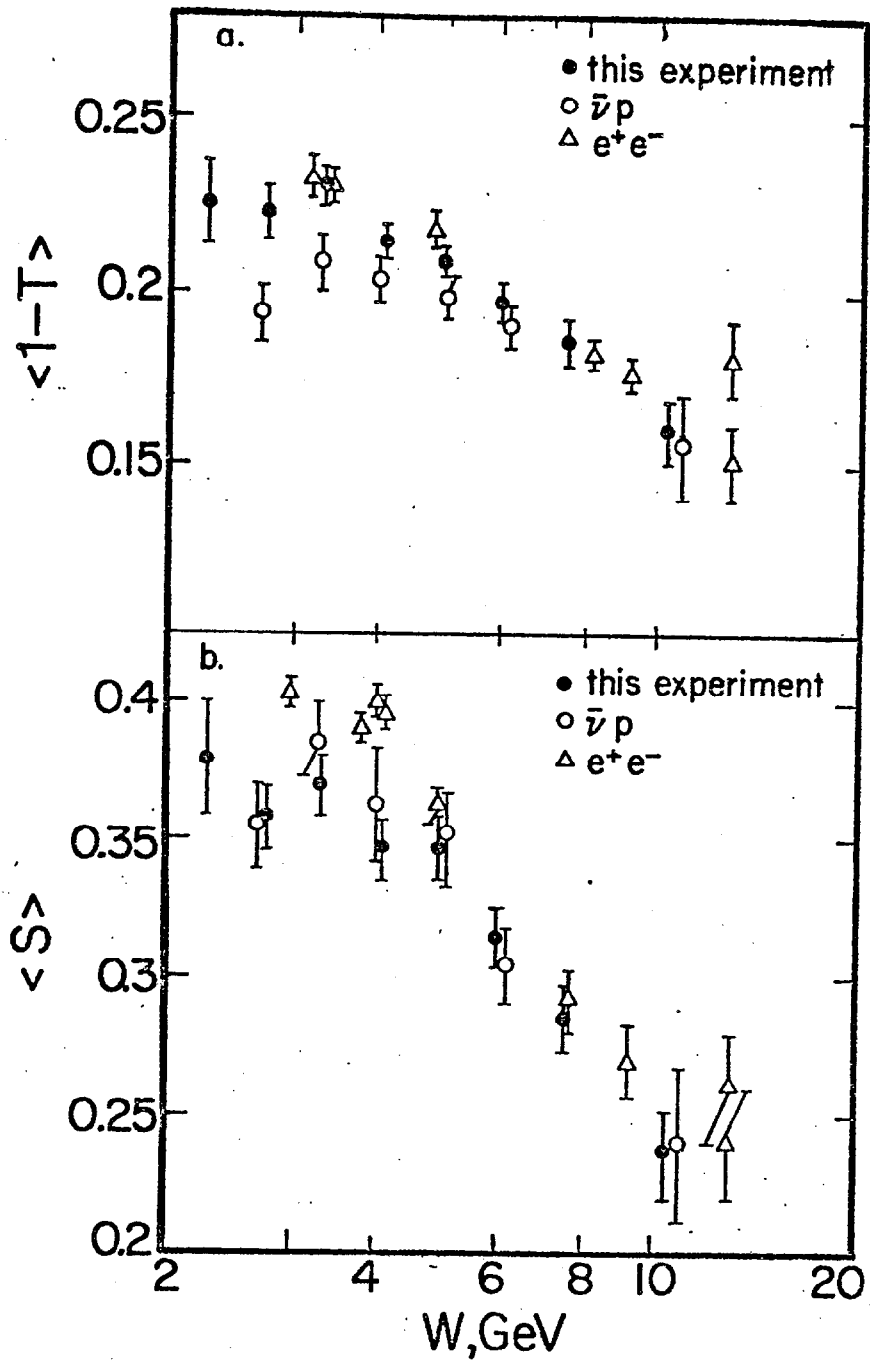


Fig. 7

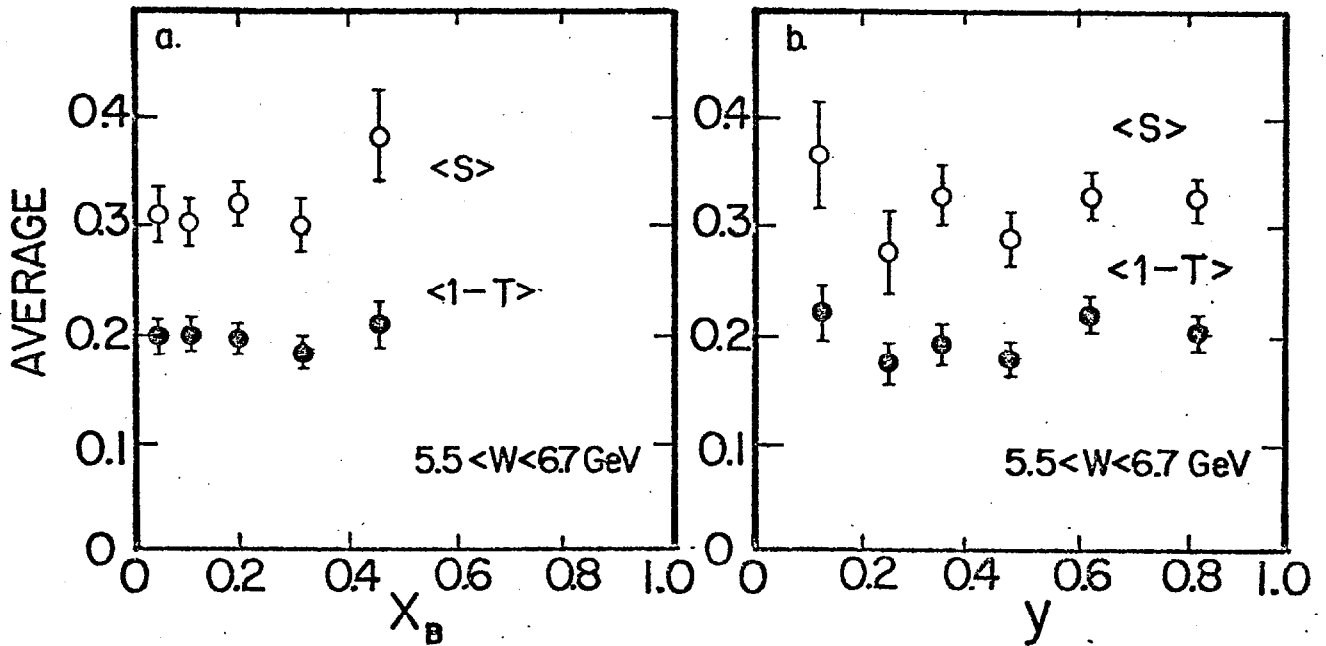


Fig. 8

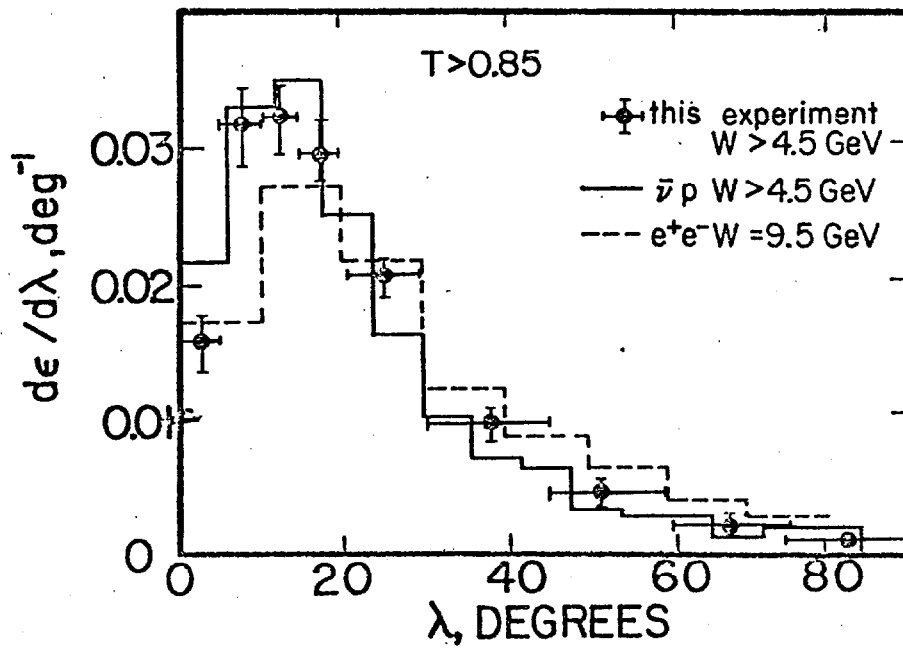


Fig. 9

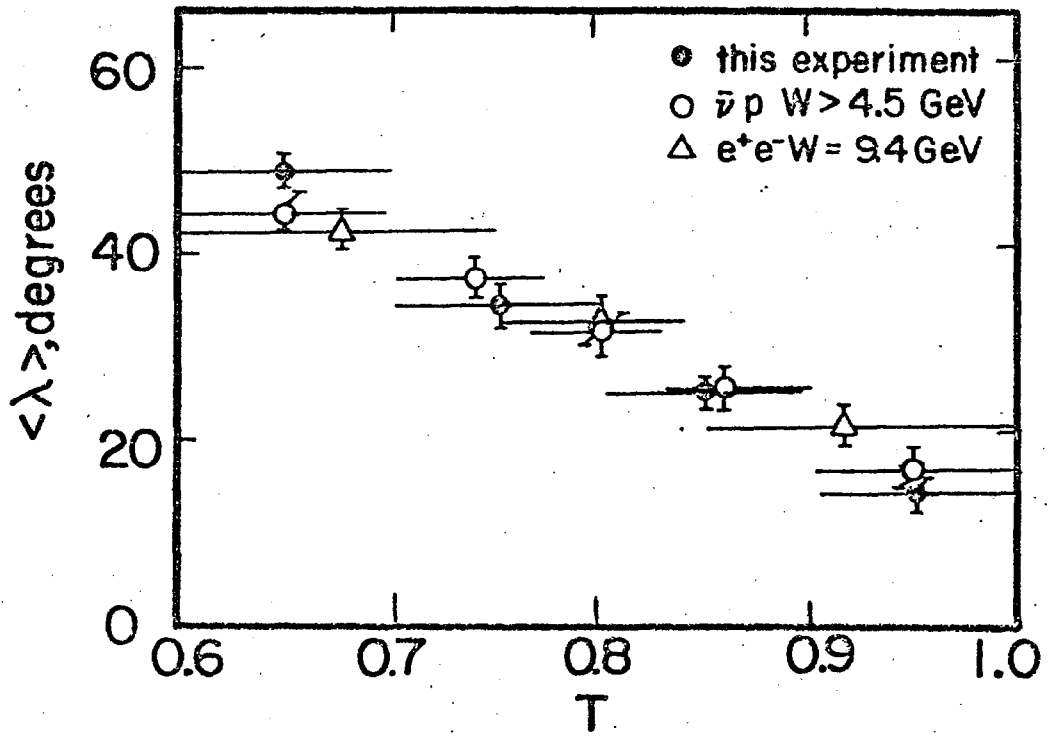


Fig. 10